

**NANO EXPRESS**

**Open Access**

# Synthesis of Gd<sub>2</sub>O<sub>3</sub>:Eu nanoplatelets for MRI and fluorescence imaging

Nabil M Maalej<sup>1,2\*</sup>, Ahsanulhaq Qurashi<sup>1,3</sup>, Achraf Amir Assadi<sup>4</sup>, Ramzi Maalej<sup>4</sup>, Mohammed Nasiruzzaman Shaikh<sup>1</sup>, Muhammad Ilyas<sup>1</sup> and Mohammad A Gondal<sup>1,2</sup>

## Abstract

We synthesized Gd<sub>2</sub>O<sub>3</sub> and Gd<sub>2</sub>O<sub>3</sub> doped by europium (Eu) (2% to 10%) nanoplatelets using the polyol chemical method. The synthesized nanoplatelets were characterized by X-ray diffraction (XRD), FESEM, TEM, and EDX techniques. The optical properties of the synthesized nanoplatelets were investigated by photoluminescence spectroscopy. We also studied the magnetic resonance imaging (MRI) contrast enhancement of T1 relaxivity using 3 T MRI. The XRD for Gd<sub>2</sub>O<sub>3</sub> revealed a cubic crystalline structure. The XRD of Gd<sub>2</sub>O<sub>3</sub>:Eu<sup>3+</sup> nanoplatelets were highly consistent with Gd<sub>2</sub>O<sub>3</sub> indicating the total incorporation of the Eu<sup>3+</sup> ions in the Gd<sub>2</sub>O<sub>3</sub> matrix. The Eu doping of Gd<sub>2</sub>O<sub>3</sub> produced red luminescence around 612 nm corresponding to the radiative transitions from the Eu-excited state <sup>5</sup>D<sub>0</sub> to the <sup>7</sup>F<sub>2</sub>. The photoluminescence was maximal at 5% Eu doping concentration. The stimulated CIE chromaticity coordinates were also calculated. Judd-Ofelt analysis was used to obtain the radiative properties of the sample from the emission spectra. The MRI contrast enhancement due to Gd<sub>2</sub>O<sub>3</sub> was compared to DOTAREM commercial contrast agent at similar concentration of gadolinium oxide and provided similar contrast enhancement. The incorporation of Eu, however, decreased the MRI contrast due to replacement of gadolinium by Eu.

**Keywords:** Rare earth nanoparticles; MRI contrast; Photoluminescent nanoparticles

## Background

Gadolinium is a rare earth (RE) metal that has paramagnetic properties that enhance the magnetic resonance imaging (MRI) signal [1]. Gadolinium ions have seven unpaired electrons in the valence shell and hence have a high magnetic moment suitable for MRI. Gadolinium accelerates proton relaxation and hence shortens the T1 relaxation time. Gadolinium complexes such as Gd-DTPA and Gd-DOTA are some of the most commonly used clinical MRI contrast agents [2,3]. Gadolinium is a good host material for luminescence applications due to its thermal, chemical, and photochemical stability [4-6].

The gadolinium oxide doped with Eu<sup>3+</sup> (Gd<sub>2</sub>O<sub>3</sub>:Eu<sup>3+</sup>) is paramagnetic with attractive photoluminescence (PL) properties. It is widely used in fluorescence lamps, television tubes, biological fluorescent labeling [5,7,8], MRI contrast [9-11], hyperthermia [12], immunoassays [13,14],

and display applications [15-18]. Eu<sup>3+</sup>-doped Gd<sub>2</sub>O<sub>3</sub> nanoparticles are red-emitting phosphors with bright luminescence and long-term photothermal stability [19]. Gd<sub>2</sub>O<sub>3</sub>:Eu<sup>3+</sup> is also a very efficient X-ray and thermoluminescent phosphor [20]. Eu<sup>3+</sup>-doped CaF<sub>2</sub>-fluorophosphate glass composites has intense IR fluorescence and is a promising candidate for IR lasers and amplifiers [21].

Gadolinium oxide and RE gadolinium oxide have been synthesized by many groups using different techniques such as sol-gel [22], polyol [23], flame-spray pyrolysis [24,25], laser ablation [26], hydrothermal [17,27,28], and direct precipitation [29].

In the present work, Gd<sub>2</sub>O<sub>3</sub> and Gd<sub>2</sub>O<sub>3</sub>:Eu<sup>3+</sup> nanoplatelets were synthesized using the simple and novel polyol chemical method. Detailed structural analysis such as field emission scanning electron microscopy (FESEM), transmission electron microscopy (TEM), and energy-dispersive X-ray EDX are reported. The photoluminescent properties of Eu<sup>3+</sup>-activated gadolinium oxide were investigated. Judd-Ofelt analysis was used to determine the radiative properties of the synthesized nanoparticles

\* Correspondence: maalej@kfupm.edu.sa

<sup>1</sup>Center of Excellence in Nanotechnology, Research Institute, King Fahd University of Petroleum and Minerals, Dhahran 31261, Saudi Arabia

<sup>2</sup>Physics Department, King Fahd University of Petroleum and Minerals, Dhahran 31261, Saudi Arabia

Full list of author information is available at the end of the article

from their PL emission spectra. The attractive multifunctional  $\text{Gd}_2\text{O}_3$  and  $\text{Gd}_2\text{O}_3:\text{Eu}^{3+}$  nanoplatelets were investigated for MRI contrast enhancement.

## Methods

### Synthesis of $\text{Gd}_2\text{O}_3$ and $\text{Gd}_2\text{O}_3:\text{Eu}^{3+}$

All reagents were of analytical grade and were used without further purification in the experiment. In this experiment, 0.5 M gadolinium acetate ( $\text{Gd}(\text{OAc})_3$ ) was dissolved in ethanol under continuous stirring. Then 50 wt.% polyethylene glycol (mol. wt 600) was transferred in the solution under continuous stirring. After some time, dropwise addition of 0.1 M diethylamine was carried out into the reaction solution. For the doping purpose, 2% Eu ( $\text{EuCl}_3$ ) was transferred in the solution. The resultant solution was refluxed at  $100^\circ\text{C}$  for 48 h. After the reaction, the flask was cooled to room temperature. The precipitates of  $\text{Gd}_2\text{O}_3$  were separated from the solution by centrifuging for 30 min with a rotation speed of 3,000 rpm and then washed using deionized water. The rinsing was repeated three to five times to totally remove organic and inorganic ions adsorbed on the surface of the product. The white grayish color product was dried in an oven at  $80^\circ\text{C}$  for 24 h. In order to obtain highly crystalline nature of  $\text{Eu-Gd}_2\text{O}_3$ , the product was further calcinated in ambient atmosphere at approximately  $600^\circ\text{C}$  for 12 h. Similar procedure was adopted for 5% and 10% europium (Eu) doping.

### Characterization

The synthesized products were characterized using X-ray diffraction (XRD), FESEM, TEM, PL, and MRI. The crystal structure of the synthesized nanoparticles was investigated by XRD using a (XRD Shimadzu 6000; Shimadzu, Kyoto, Japan) advance X-ray diffractometer with  $\text{Cu-K}\alpha$  radiation source ( $\lambda = 1.5418 \text{ \AA}$ ). The FESEM analysis was done using (FESEM JSM-6700F). TEM analysis was done on a high-resolution transmission electron microscope (HRTEM; JEOL, Tokyo, Japan). The PL spectrum was recorded using Shimadzu spectrofluorometer (Shimadzu). The excitation source was a 150-W Xenon lamp with excitation wavelength fixed at 350 nm, and the emission monochromator was scanned in the 450 to 900-nm wavelength range. The MRI contrast enhancement due to different  $\text{Gd}_2\text{O}_3$  concentrations from a commercial contrast agent, Dotarem<sup>®</sup> (Guerbet LLC, Bloomington, IN, USA), was compared to the contrast due to  $\text{Gd}_2\text{O}_3$  nanoparticles and  $\text{Gd}_2\text{O}_3$  nanoparticles doped with Eu (2% to 10%). The different concentrations were placed in plastic 10 ml test tubes. The test tubes were placed in a plastic test tube holder and imaged in a 3 T MRI scanner (General Electric, Fairfield, CT, USA). A pulse echo T1 sequence was used with pulse repetition rates of 20, 30, 50, 100, 200, 300, 400, 500, and 1,000 ms. The images were then analyzed in

order to determine the contrast enhancement due to the nanoparticles and to obtain the T1 relaxation times.

## Results and discussion

### Structural properties

XRD measurements were used to explore the phase and structure of  $\text{Gd}_2\text{O}_3$  and  $\text{Gd}_2\text{O}_3:\text{Eu}^{3+}$  nanostructures. Figure 1a demonstrates the XRD pattern of  $\text{Gd}_2\text{O}_3$  and 2%, 5%, and 10%  $\text{Gd}_2\text{O}_3:\text{Eu}^{3+}$ , respectively. These results confirmed the cubic structure of  $\text{Gd}_2\text{O}_3$  and  $\text{Gd}_2\text{O}_3:\text{Eu}^{3+}$  with spatial group Ia3 (JCPDS card No. 00-012-0797). No other peaks were observed in the XRD spectrum related to impurities. Due to Eu doping, a high-intensity (222) peak shift was observed as shown in Figure 1b. The presence of strong peaks indicates the highly crystalline nature of  $\text{Gd}_2\text{O}_3$  nanostructures.

Figure 2a,b,c,d shows the FESEM images of  $\text{Gd}_2\text{O}_3$  and  $\text{Gd}_2\text{O}_3:\text{Eu}^{3+}$  with different doping concentrations of 2%, 5%, and 10%, respectively. Figure 2a shows fine nanoflakes of  $\text{Gd}_2\text{O}_3$ . It is interesting to note that the

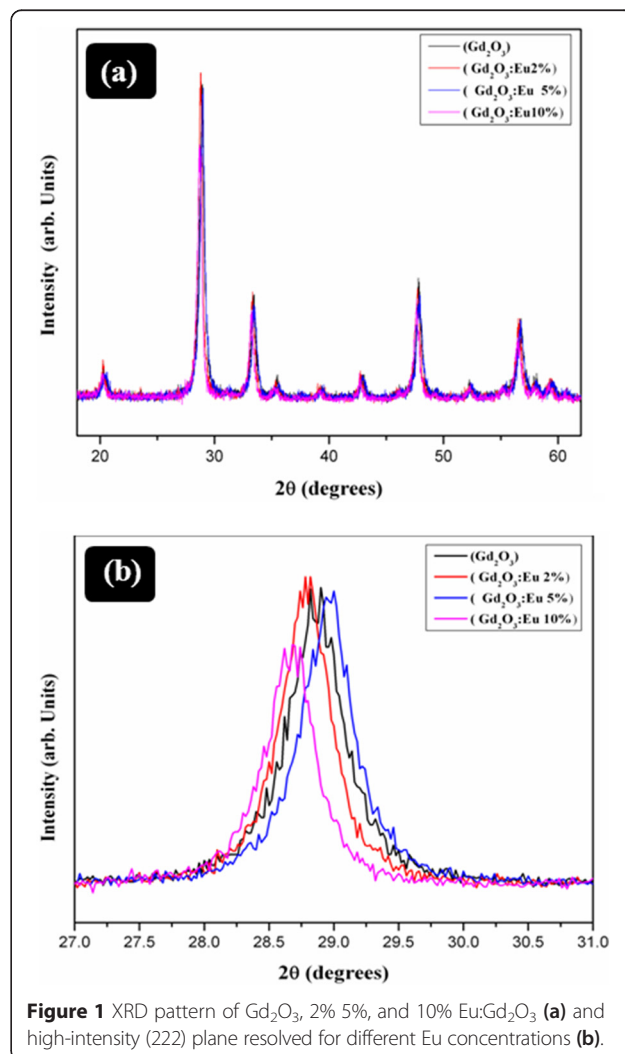


**Figure 1** XRD pattern of  $\text{Gd}_2\text{O}_3$ , 2% 5%, and 10%  $\text{Eu}:\text{Gd}_2\text{O}_3$  (a) and high-intensity (222) plane resolved for different Eu concentrations (b).

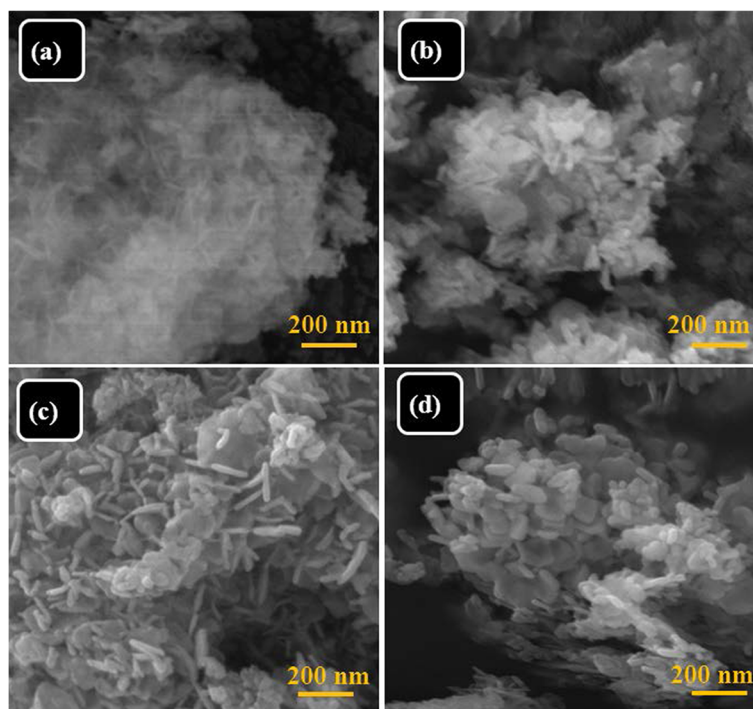


**Figure 2** FESEM micrograph of (a)  $\text{Gd}_2\text{O}_3$ , (b)  $\text{Gd}_2\text{O}_3:\text{Eu}$  2%, (c)  $\text{Gd}_2\text{O}_3:\text{Eu}$  5%, and (d)  $\text{Gd}_2\text{O}_3:\text{Eu}$  10%.

thickness of the nanostructures augmented when doped with 2% Eu. Figure 2b shows FESEM micrograph of 2%  $\text{Gd}_2\text{O}_3:\text{Eu}^{3+}$  nanoplatelets with some nanocrystals. When the concentration of  $\text{Eu}^{3+}$  increased to 5%, highly uniform nanoplatelets were formed. The thickness of each nanoplatelet is about 15 to 25 nm (Figure 2c). Figure 2d shows FESEM micrograph of 10%  $\text{Gd}_2\text{O}_3:\text{Eu}^{3+}$  irregularly thick nanoplatelets. It is observed that by further increasing the concentration of Eu, the thickness and diameter of nanoplatelets increased significantly. FESEM observation showed clear change in the morphology due to doping from  $\text{Gd}_2\text{O}_3$  nanoflakes to thick  $\text{Gd}_2\text{O}_3:\text{Eu}^{3+}$  nanoplatelets.

Figure 3a,b,c,d,e,f,g,h shows TEM HRTEM images of  $\text{Gd}_2\text{O}_3$  with different Eu concentrations (2%, 5%, and 10%). The TEM analysis is in agreement with FESEM results in which the evolution of nanoplatelets is observed. The growth of  $\text{Gd}_2\text{O}_3:\text{Eu}^{3+}$  nanoplatelets is seen in TEM micrographs. From the HRTEM, the interspacing between the lattice fringes was found to be 0.316 nm which corresponds to growth plane (110) indicating the growth of nanoplatelets along the axis in [001] direction. The energy-dispersive spectrum (EDS) investigation (Figure 4) also confirmed that all the detected peaks are related to Gd, O, and Eu, indicating a chemically pure  $\text{Gd}_2\text{O}_3:\text{Eu}^{3+}$  phase. No other peak related to impurities was found in the samples.

### Fluorescence properties

Figure 5 shows the PL spectra of  $\text{Eu}^{3+}$ -doped  $\text{Gd}_2\text{O}_3$  nanoparticles for different dopant concentrations (2%, 5%, and 10%) recorded in the 450 to 900-nm wavelength range. The spectra have five emission lines at 580, 593, 612, 652, and 708 nm corresponding to  $^5\text{D}_0 \rightarrow ^7\text{F}_J$  ( $J = 0, 1, 2, 3, 4$ ) transitions, respectively. The two transitions corresponding to  $^5\text{D}_0 \rightarrow ^7\text{F}_J$  ( $J = 5, 6$ ) are presented in the inset of Figure 5. We recorded a strong PL peak centered around 612 nm in addition to many smaller peaks for three different concentrations of Eu in  $\text{Gd}_2\text{O}_3$ . The high red luminescence signal intensity for Eu-doped samples around 612 nm corresponds to the radiative transitions from the Eu-excited state  $^5\text{D}_0$  to the  $^7\text{F}_2$  state (Figure 5). This sharp intense line indicates a complete incorporation of the dopant ions into  $\text{Gd}_2\text{O}_3$  nanocrystals by replacing  $\text{Gd}^{3+}$  in a preferred  $\text{C}_2$  site symmetry compared to the  $\text{S}_6$  symmetry indicated by the  $^5\text{D}_0$  to the  $^7\text{F}_1$  transition [30]. In addition to the intense peak, numerous smaller peaks have been identified in the visible spectral range between 500 and 800 nm corresponding to the transitions from excited to the ground energy level of Eu. We also observed an increase of the emission intensities when the  $\text{Eu}^{3+}$  concentration increases to reach a maximal value at 5 mol%. Then the emission intensities decrease because of the concentration quenching. This emission behavior resembles exactly the fluorescence of  $\text{Eu}^{3+}$ -doped phosphors [29,31].

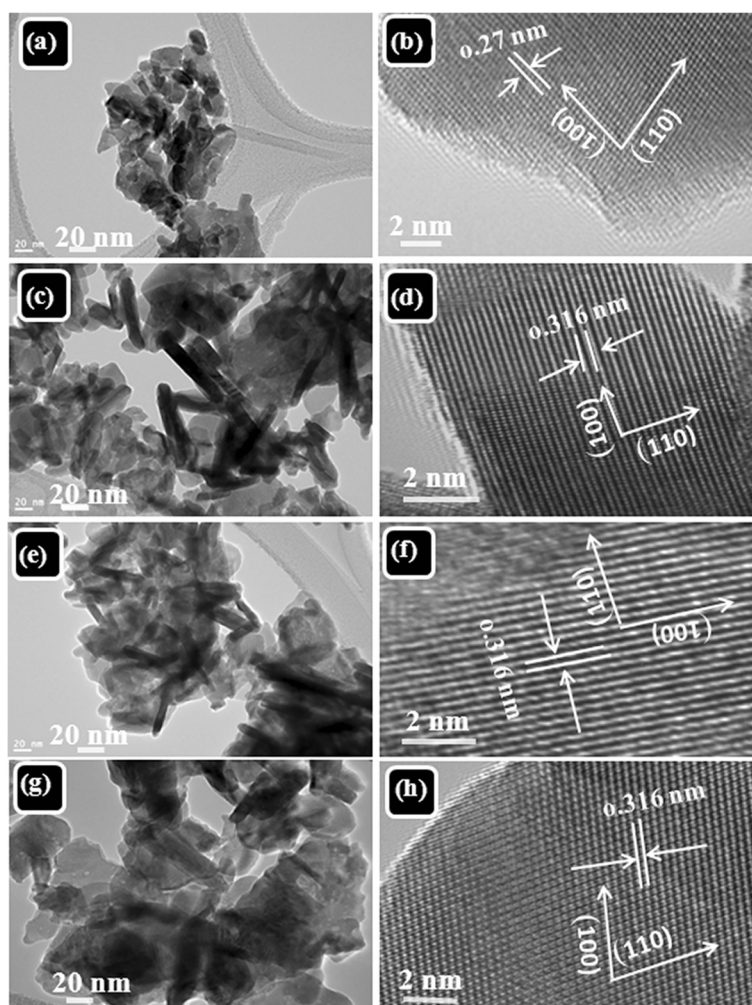


**Figure 3** TEM micrographs of (a,b)  $\text{Gd}_2\text{O}_3$ , (c,d)  $\text{Gd}_2\text{O}_3:\text{Eu}$  2%, (e,f)  $\text{Gd}_2\text{O}_3:\text{Eu}$  5%, and (g,h)  $\text{Gd}_2\text{O}_3:\text{Eu}$  10%.

Based on these measurements, we deduced an energy level scheme (Grotrian diagram) of the observed transition in PL spectra as shown in Figure 6 and Table 1.

#### CIE chromaticity coordinates

The luminescent intensity of the emission spectral measurements has been characterized using the CIE1931 chromaticity diagram (Figure 7) to get information about the composition of all colors on the basis of color matching functions  $\bar{x}(\lambda)$ ,  $\bar{y}(\lambda)$ , and  $\bar{z}(\lambda)$  [32,33]. The  $(x, y)$  coordinates are used to represent the color and locus of all the monochromatic color coordinates. The values of the color chromaticity coordinates  $(x, y)$  were found to be  $(x = 0.6387; y = 0.3609)$  for  $\text{Gd}_2\text{O}_3:\text{Eu}^{3+}$  (2%),  $(x = 0.6447; y = 0.3550)$  for  $\text{Gd}_2\text{O}_3:\text{Eu}^{3+}$  (5%), and  $(x = 0.6477; y = 0.3520)$  for  $\text{Gd}_2\text{O}_3:\text{Eu}^{3+}$  (10%) (Figure 7). The color coordinates are all in the pure red region of the chromaticity diagram. Indeed, the present nanoplatelets

$\text{Gd}_2\text{O}_3:\text{Eu}^{3+}$  give emission in the red region with appreciable intensity for fluorescence imaging.

#### Judd-Ofelt and radiative analysis

The Judd-Ofelt theory [34,35] is the most widely used and known theory in the analysis of spectroscopic properties of rare earth ions in different hosts. The great appeal of this theory is the ability to forecast the oscillator strengths in absorption and to give information about the luminescence branching ratios and lifetimes by using only three parameters,  $\Omega_k$  ( $k = 2,4,6$ ) [36-39].

For the particular Eu rare earth ion-doped materials, the J-O intensity parameters are calculated with two different methods. The first method is based on the optical absorption spectra. The second method is referred to the analysis of emission spectra at room temperature. It is noteworthy to mention that in the case of  $\text{Eu}^{3+}$ -doped nontransparent hosts, we are not always able to measure the absorption spectra [40,41]. Therefore, for



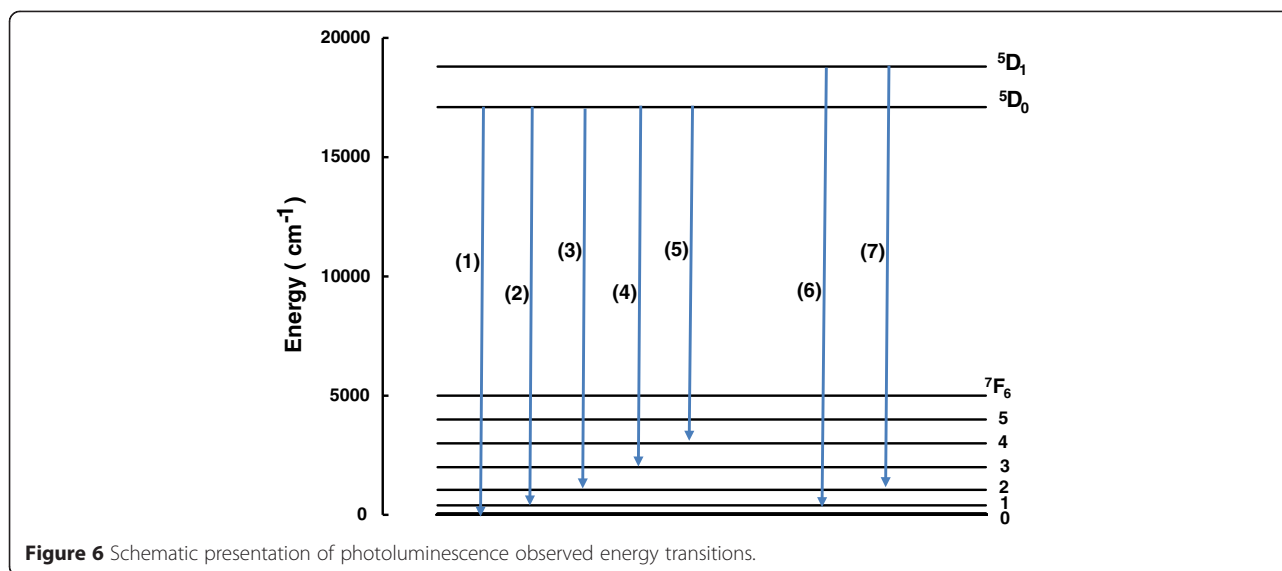


**Figure 6** Schematic presentation of photoluminescence observed energy transitions.

the magnetic dipole radiative transition rates  $A^{md}$  can be evaluated using the following expression:

$$A_{J-J'}^{md} = \frac{64\pi^4 \nu_{md}^3}{3h(2J+1)} n^3 S_{md}$$

Where  $n$  is the refractive index,  $(2J+1)$  is the degeneracy of the initial state  $J$  and  $\nu_{md}$  is the transition energy of the  ${}^5D_0 \rightarrow {}^7F_1$  transition ( $\text{cm}^{-1}$ ),  $h$  is Planck constant ( $6.63 \times 10^{-27}$  erg s).  $S_{md}$  is the magnetic dipolar transition line strength, which is independent of host matrix and is equal to  $11.26 \times 10^{-42}$  (esu)<sup>2</sup>  $\text{cm}^2$  [42]. From the definition of the  $A_{J-J'}^{md}$ , the refractive index can be calculated to be 1.58.

For a particular transition, the intensity ( $I$ ) of an emission transition is proportional to the radiative decay rate  $A_{J-J'}^{ed}$ , of that transition, which equals the reciprocal of intrinsic lifetime  $\tau_0$ . The intensity is also proportional to the area under that emission curve [43]. Thus, the intensity of an emission transition can be written as [44] follows:

**Table 1** Photoluminescence transitions observed for  $\text{Gd}_2\text{O}_3:\text{Eu}^{3+}$  nanoplatelets

label	Wavelength (nm)	Transition from	To
1	580	${}^5D_0 \rightarrow$	${}^7F_0$
2	593	${}^5D_0 \rightarrow$	${}^7F_1$
3	612	${}^5D_0 \rightarrow$	${}^7F_2$
4	652	${}^5D_0 \rightarrow$	${}^7F_3$
5	708	${}^5D_0 \rightarrow$	${}^7F_4$
6	538	${}^5D_1 \rightarrow$	${}^7F_1$
7	554	${}^5D_1 \rightarrow$	${}^7F_2$

$$I = \eta \sum_{j'=0,1\dots 6} A_{7F_{j'}}^{ed}$$

The fluorescence lifetime of the nanoparticles is approximately 1 ms [45,46]. The values of  $A_{7F_{j'}}$ , shown in Table 2 were determined by calculating the constant  $\eta$ . The radiative branching ratio shown in Table 2 was calculated using  $\beta_{J-J'} = \frac{A_{J-J'}}{\sum_{j'=0,1\dots 6} A_{7F_{j'}}$

The electric dipole transitions  ${}^5D_0 \rightarrow {}^7F_{J'}$  ( $J' = 2, 4,$  and  $6$ ) can be represented by using the three J-O parameters  $\Omega_k$  ( $k = 2, 4, 6$ ) as follows [47,48]:

$$A_{J-J'}^{ed} = \frac{64\pi^4 e^2 \nu^3 n(n^2 + 2)2}{27h(2J+1)} \sum_{k=2,4,6} \Omega_k |\psi_J |U^{(k)}| \psi_{J'}|^2$$

where  $h$  is the Planck's constant,  $\nu$  is the transition energy of electric dipole transition (in  $\text{cm}^{-1}$ ) and  $e$  is the charge of an electron, and  $|\langle {}^5D_0 |U^{(k)}| {}^7F_{J'} \rangle|^2$  is the double-reduced matrix element. All of the matrix elements for  ${}^5D_0 \rightarrow {}^7F_{J'}$  transitions are zero [49-51], except those for the  ${}^5D_0 \rightarrow {}^7F_2$  transition ( $U^{(2)} = 0.0028$ ), the  ${}^5D_0 \rightarrow {}^7F_4$  transition ( $U^{(4)} = 0.002$ ) and the  ${}^5D_0 \rightarrow {}^7F_6$  transition ( $U^{(6)} = 0.0002$ ). Thus, the values of  $\Omega_k$  can be calculated using the emissions of  ${}^5D_0 \rightarrow {}^7F_{J'}$  ( $J' = 2, 4, 6$ ). The results of our calculations are shown in Table 3 together with the  $\Omega_k$  values of  $\text{Eu}^{3+}$  ions in other hosts [41,51-57].

These intensity parameters follow the tendency  $\Omega_2 > \Omega_4 > \Omega_6$  found for other materials containing  $\text{Eu}^{3+}$  ions. It is well known that  $\Omega_2$  is most sensitive to the local structure and its value is indicative the higher asymmetry and higher covalence around the  $\text{Eu}^{3+}$  ions with their surrounding ligands [58]. However, the parameter  $\Omega_6$  is inversely proportional to the Eu-O band covalency, since it

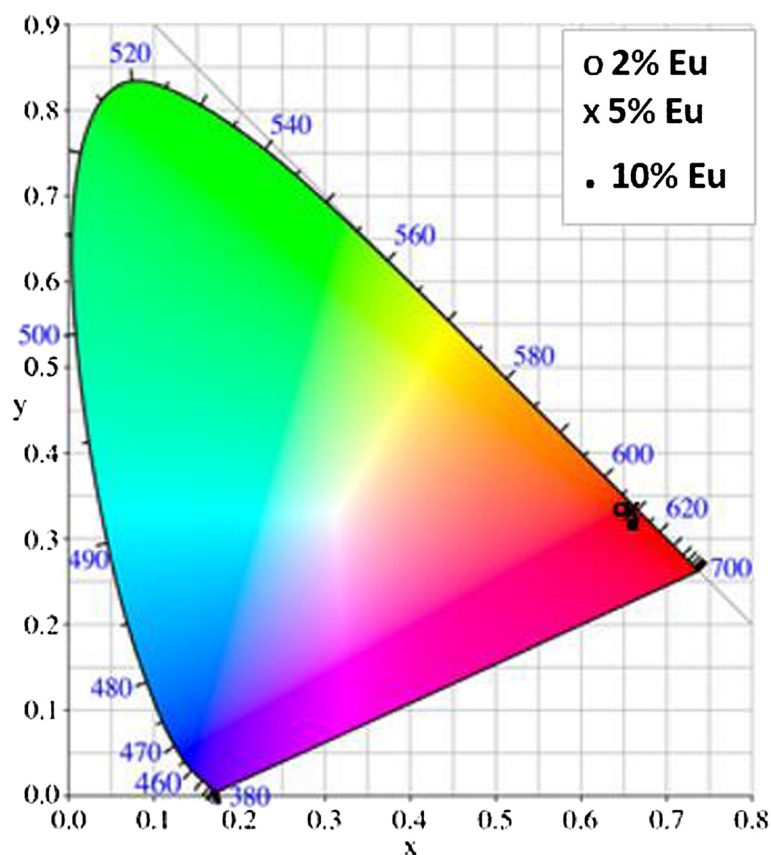


**Figure 7** The CIE coordinate for  $\text{Eu}^{3+}$ -doped  $\text{Gd}_2\text{O}_3$  upon excitation at 365 nm.

is more strongly affected by the overlap integrals of 4f and 5d orbitals than  $\Omega_2$  and  $\Omega_4$  [58].

**The MRI contrast enhancement**

We have tested MR image enhancement properties of the gadolinium nanoparticles and the Eu-doped nanoparticles using the MRI scanner at King Fahd Specialist Hospital. We also compared the MR images to commercially available

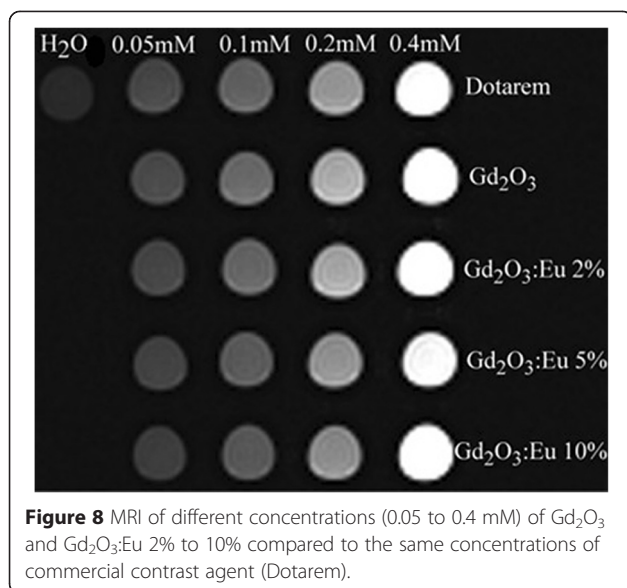
MRI contrast agent (DOTAREM) using the same gadolinium concentrations (Gd molar concentrations 0.05, 0.1, 0.2 and 0.4 mM). The gadolinium oxide nanoparticles provided comparable MR image enhancement to the commercially used contrast agent DOTAREM (Figure 8). The addition of

**Table 2** Wavenumbers, transition rates, and branching ratio for  $^5D_0 \rightarrow ^7F_J (J = 0 - 6)$  of  $\text{Eu}^{3+}$  ions in  $\text{Gd}_2\text{O}_3$

Transition	Type	Wavenumber ( $\text{cm}^{-1}$ )	Transition rate ( $\text{s}^{-1}$ )	Branching ratio $\beta$ (%)
$^5D_0 \rightarrow ^7F_0$	Forbidden	17,241	19.1132	1.9109
$^5D_0 \rightarrow ^7F_1$	Magnetic dipole	16,863.4	66.5612	6.6548
$^5D_0 \rightarrow ^7F_2$	Electric dipole	16,339	876.9950	87.6820
$^5D_0 \rightarrow ^7F_3$	Forbidden	15,337	10.0094	1.0007
$^5D_0 \rightarrow ^7F_4$	Electric dipole	14,124	27.0115	2.7006
$^5D_0 \rightarrow ^7F_5$	Forbidden	13,422	0.4321	0.0432
$^5D_0 \rightarrow ^7F_6$	Electric dipole	12,422	0.0534	0.0053

**Table 3** J-O parameters of  $\text{Eu}^{3+}$  in several compounds

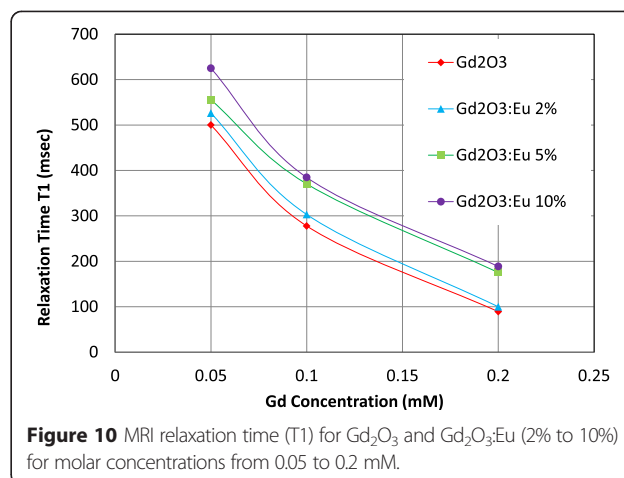
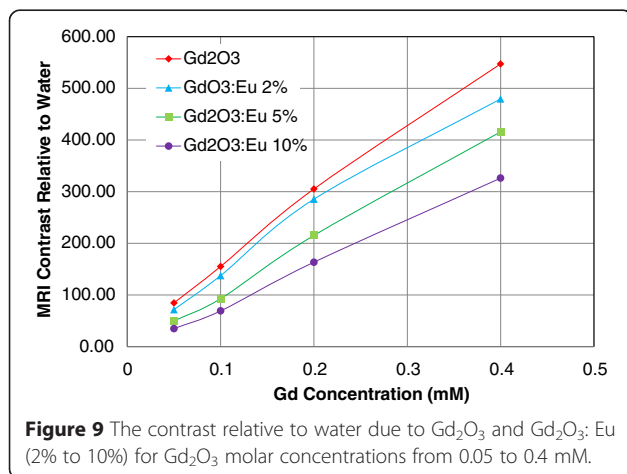
Compounds	$\Omega_2$ ( $10^{-20} \text{ cm}^2$ )	$\Omega_4$ ( $10^{-20} \text{ cm}^2$ )	$\Omega_6$ ( $10^{-20} \text{ cm}^2$ )	Reference
$\text{Gd}_2\text{O}_3:\text{Eu}^{3+}$ nanoplatelets	28.07	1.87	0.05	This work
KLTB: $\text{Eu}^{3+}$	14.20	~0	2.40	Saleem (2010) [54]
L4BE: $\text{Eu}^{3+}$	17.56	~0	4.26	Babu (2000) [55]
LaOF: $\text{Eu}^{3+}$	56.3	13.9	-	Grzyb (2011) [56]
$\text{Gd}_2\text{O}_3:\text{Eu}^{3+}$ nanocrystals	5.61	1.57	-	Liu (2006) [57]
$\text{Eu}_{0.08}\text{K}_{0.075}\text{Ba}_{0.845}\text{TiO}_3$	6.92	1.84	-	Li (2008) [53]
$\text{Gd}_2(\text{W}_{0.5}\text{Mo}_{0.5})\text{O}_6:\text{Eu}^{3+}$	6.91	0.22	-	Yue (2011) [41]
Fluorosilicate glass ceramic	1.38	0.84	-	Zhao (2007) [52]
Fluorophosphate glass	3.24	5.11	2.89	Balda (1996) [51]



Eu reduced the MRI contrast due to the replacement of gadolinium atoms by the Eu atoms in the material structure. Figure 9 shows the contrast relative to water due to Dotarem,  $Gd_2O_3$ , and  $Gd_2O_3:Eu$  (2% to 10%) for Gd molar concentration from 0.05 to 0.4 mM. Figure 10 shows the variation of the T1 relaxation time for Dotarem,  $Gd_2O_3$ , and  $Gd_2O_3:Eu$  (2% to 10%) for Gd molar concentration from 0.05 to 0.2 mM.

### Conclusions

We synthesized nanoplatelets of  $Gd_2O_3$  and  $Gd_2O_3:Eu^{3+}$  (2%, 5%, and 10%). The doping with Eu preserved the crystalline cubic structure of the  $Gd_2O_3$  matrix. The MRI contrast of the  $Gd_2O_3$  was comparable to the commercial gadolinium-based contrast agent DOTAREM at the same gadolinium concentrations. Doping the  $Gd_2O_3$  with Eu exhibits very strong PL spectra especially in the red region at 612 nm corresponding to the radiative



transitions from the Eu-excited state  $^5D_0$  to the  $^7F_2$  state. The strongest red PL was obtained at 5% Eu doping concentration. The stimulated CIE chromaticity coordinates and Judd-Ofelt analysis were used to obtain the radiative properties of the sample from the emission spectra. However, doping with Eu has decreased the MRI contrast and increased the T1 relaxation time. The MRI contrast enhancement decreased with increasing Eu doping concentration due to the replacement of the gadolinium atoms with Eu. The synthesized nanoparticles can be used as a contrast agent for magnetic resonance imaging. The PL in the red region can be exploited in labeling biological materials for fluorescence microscopy applications. The synthesized nanoplatelets have to be coated or encapsulated in biocompatible material such as polyethylene glycol to be used for *in vivo* MRI of cancer tissues with or without targeting molecules.

### Competing interests

The authors declare that they have no competing interests.

### Authors' contributions

NM coordinated the project, conducted the MRI testing and analysis, and drafted the paper. AQ was in charge of nanoparticle synthesis, the TEM analysis, and contributed to writing the paper. AA did the Judd-Ofelt analysis of the PL spectra and contributed to the paper writing. RM was in charge the spectroscopic analysis, the PL emission spectra, the stimulated CIE chromaticity analysis, and Judd-Ofelt analysis, and contributed to the writing of the paper. NS was in charge of nanoparticle characterization including FESEM and XRD analyses. MI did the day-to-day experiments in synthesis and contributed to the nanoparticle characterization. MG was in charge of the PL spectroscopy and analysis and contributed to the writing of the paper. All authors read and approved the final manuscript.

### Acknowledgements

The author(s) would like to acknowledge the support provided by King Abdulaziz City for Science and Technology (KACST) through the Science & Technology Unit at King Fahd University of Petroleum & Minerals (KFUPM) for funding this work through project No. 10-NAN1386-04 as part of the National Science, Technology and Innovation Plan. We also would like to acknowledge the MRI support we received from Mr. Mustafa Al Muqbel from King Fahad Specialist Hospital, Dammam, KSA.

**Author details**

<sup>1</sup>Center of Excellence in Nanotechnology, Research Institute, King Fahd University of Petroleum and Minerals, Dhahran 31261, Saudi Arabia. <sup>2</sup>Physics Department, King Fahd University of Petroleum and Minerals, Dhahran 31261, Saudi Arabia. <sup>3</sup>Chemistry Department, King Fahd University of Petroleum and Minerals, Dhahran 31261, Saudi Arabia. <sup>4</sup>Laboratoire Géosciences, Matériaux, Environnement et Changements Globaux, Faculté des Sciences de Sfax, Université de Sfax, Sfax 3018, Tunisia.

Received: 17 December 2014 Accepted: 16 April 2015

Published online: 13 May 2015

**References**

- Thompson CC. Gadolinium: compounds, production and applications. Edited by Thompson CC. New York: Nova Science Pub Inc; 2011.
- Caravan P, Ellison JJ, McMurry TJ, Lauffer RB. Gadolinium(III) chelates as MRI contrast agents: structure, dynamics, and applications. *Chem Rev*. 1999;99:2293.
- Geraldes CF, Laurent S. Classification and basic properties of contrast agents for magnetic resonance imaging contrast media. *Mol Imaging*. 2009;4:1.
- Zhou Y, Lin J, Wang S. Energy transfer and upconversion luminescence properties of  $Y_2O_3:Sm$  and  $Gd_2O_3:Sm$  phosphors. *J Solid State Chem*. 2003;171:391.
- Lu H, Yi G, Zhao S, Chen D, Guo LH, Cheng J. Synthesis and characterization of multi-functional nanoparticles possessing magnetic up-conversion fluorescence and bio-affinity properties. *Mater Chem*. 2004;14:1336.
- Hirai T, Orikoshi T. Preparation of  $Gd_2O_3:Yb$ , Er and  $Gd_2O_3:Yb$ , Er infrared-to-visible conversion phosphor ultrafine particles using an emulsion liquid membrane system. *J Colloid Interface Sci*. 2004;269:103–8.
- Anker JN, Kopelman R. Magnetically modulated optical nanoprobe. *Appl Phys Lett*. 2003;82:1102.
- Lechevallier SV, Lecante P, Mauricot R, Dexpert H, Dexpert-Ghys J, Kong HK, et al. Gadolinium–Europium carbonate particles: controlled precipitation for luminescent biolabeling. *Chem Mater*. 2010;22:6153.
- Lee JE, Lee N, Kim H, Kim J, Choi SH, Kim JH, et al. Uniform mesoporous dye-doped silica nanoparticles decorated with multiple magnetite nanocrystals for simultaneous enhanced magnetic resonance imaging, fluorescence imaging, and drug delivery. *J Am Chem Soc*. 2010;132:552–7.
- Wenlong X, Ja YP, Krishna K, Badrul Alam B, Woo CH, Seonguk J, et al. A T1, T2 magnetic resonance imaging (MRI)-fluorescent imaging (FI) by using ultrasmall mixed gadolinium–europium oxide nanoparticles. *New J Chem*. 2012;36:2361–7.
- Hu Z, Ahm M, Seleg L, Skoglund C, Sçderlind F, Engström M, et al. Highly water-dispersible surface-modified  $Gd_2O_3$  nanoparticles for potential dual-modal bioimaging. *Chem Eur J*. 2013;19:12658.
- Johannsen M, Gneveckow U, Eckelt L, Feussner A, Waldofner N, Scholz R, et al. Clinical hyperthermia of prostate cancer using magnetic nanoparticles: presentation of a new interstitial technique. *Int J Hyperthermia*. 2005;21:637.
- Feng J, Shan G, Maquieira A, Koivunen ME, Guo B, Hammock BD, et al. Functionalized europium oxide nanoparticles used as a fluorescent label in an immunoassay for atrazine. *Anal Chem*. 2003;75:5282.
- Nichkova M, Dosev D, Gee SJ, Hammock BD, Kennedy IM. Microarray immunoassay for phenoxybenzoic acid using polymer encapsulated  $Eu:Gd_2O_3$  nanoparticles as fluorescent labels. *Anal Chem*. 2005;77:6864–73.
- Blasse G, Grabmaier BC. Luminescent materials. Edited by Blasse G and Grabmaier BC. Berlin: Springer; 1994.
- Rosner W. The conversion of high energy radiation to visible light by luminescent ceramics. *IEEE Trans Nucl Sci*. 1993;40:376.
- Goldys EM, D-Tomsia K, Jinjun S, Dosev D, Kennedy IM, Yatsunenko S, et al. Optical characterization of Eu-doped and undoped  $Gd_2O_3$  nanoparticles synthesized by the hydrogen flame pyrolysis method. *J Am Chem Soc*. 2006;128:14498.
- Bedekar V, Dulta DP, Mohapatra M, Godbole SV, Ghildiyal R, Tyagi AK. Rare-earth doped gadolinia based phosphors for potential multicolor and white light emitting deep UV LEDs. *Nanotechnology*. 2009;20:5707.
- Bhargava RN. Doped nanocrystalline materials - physics and applications. *J Lumin*. 1996;70:85.
- Rosner W, Grabmaier BC. Phosphors for X-ray detectors in computed tomography. *J Lumin*. 1991;48:29.
- Jintai F, Xinqiang Y, Rihong L, Hongxing D, Jun W, Long Z. Intense photoluminescence at 2.7  $\mu m$  in transparent  $Er^{3+}:CaF_2$ -fluorophosphate glass microcomposite. *Opt Lett*. 2011;36:4347.
- Murillo AG, Ramírez AM, Romo FC, Hernández MG, Crespo MD. Synthesis, structural and optical studies of sol–gel  $Gd_2O_3:Eu^{3+}, Tb^{3+}$  films. *Mater Lett*. 2009;04:034.
- Müller A, Heim O, Panneerselvam M, Willert-Porada M. Polyol method for the preparation of nanosized  $Gd_2O_3$ , boehmite and other oxides materials. *Res Bull*. 2005;40:2153.
- Mangiarini F, Naccache R, Speghini A, Bettinelli M, Vetrone F, Capobianco JA. Upconversion in  $Er^{3+}$ -doped  $Gd_2O_3$  nanocrystals prepared by propellant synthesis and flame spray pyrolysis. *Mat Res Bull*. 2010;45:927.
- Iwako Y, Akimoto Y, Omiya M, Ueda T, Yokomori T. Photoluminescence of cubic and monoclinic  $Gd_2O_3:Eu$  phosphors prepared by flame spray pyrolysis. *J Lumin*. 2010;130:1470.
- Ledoux G, Aman D, Dujardin C, Masenelli-Varlot K. Facile and rapid synthesis of highly luminescent nanoparticles via pulsed laser ablation in liquid. *Nanotechnology*. 2009;20:5605.
- Liu G, Hong G, Wang J, Dong X. Hydrothermal synthesis of spherical and hollow  $Gd_2O_3:Eu^{3+}$  phosphors. *J Alloys Compd*. 2007;432:200.
- Kyung-Hee L, Yun-Jeong B, Song-Ho B. Nanostructures and photoluminescence properties of  $Gd_2O_3:Eu$  red-phosphor prepared via hydrothermal route. *Bull Korean Chem Soc*. 2008;29:2161.
- Bazzia R, Flores-Gonzalez MA, Louisa C, Lebboua K, Dujardina C, Breniera A, et al. Synthesis and luminescent properties of sub-5-nm lanthanide oxides nanoparticles. *J Lumin*. 2003;102:445.
- Kumar RG, Hata AS, Gopchandran KG. Diethylene glycol mediated synthesis of  $Gd_2O_3:Eu^{3+}$  nanoporphor and its Judd–Ofelt analysis. *Ceram Inter*. 2013;39:9125.
- Kang YC, Park SB, Lenggono IW, Okuyama K.  $Gd_2O_3:Eu$  phosphor particles with sphericity, submicron size and non-aggregation characteristics. *J Phys Chem Solid*. 1999;60:379.
- Harris AC, Weatherall IL. Objective evaluation of color variation in the sand-burrowing beetle *Chaerodes trachyscelides* White (Coleoptera: Tenebrionidae) by instrumental determination of CIELAB values. *J Royal Soc New Zeal*. 1990;20:253.
- Fairman HS, Brill MH, Hemmendinger H. How the CIE 1931 color-matching functions were derived from Wright-Guild data. *Color Res Appl*. 1997;22:11.
- Judd BR. Optical absorption intensities of rare-earth ions. *Phys Rev*. 1962;127:750–61.
- Ofelt GS. Intensities of crystal spectra of rare-earth ions. *J Chem Phys*. 1962;37:511–20.
- Damak K, El Sayed Y, Al-Shihri AS, Seo HJ, Rüssel C, Maalej R. Quantifying Raman and emission gain coefficients of  $Ho^{3+}$  doped  $TeO_2:ZnO:PbO:PbF_2:Na_2O$  (TZPPN) tellurite glass. *Solid State Sci*. 2014;28:7480.
- Damak K, Maalej R, Yousef ES, Qusti AH, Rüssel C. Thermal and spectroscopic properties of  $Tm^{3+}$  doped TZPPN transparent glass laser material. *J Non-Cryst Solids*. 2012;358:2974.
- Damak K, Yousef E, AlFaify S, Rüssel C, Maalej R. Raman, green and infrared emission cross-sections of  $Er^{3+}$  doped TZPPN tellurite glass. *Opt Mater Express*. 2014;4:597.
- Assadi AA, Damak K, Lachheb R, Herrmann R, Yousef E, Rüssel C, et al. Spectroscopic and luminescence characteristics of erbium doped TNZL glass for lasing materials. *J Alloy Comp*. 2015;620:129.
- Lei F, Yan B, Chen HH. Solid-state synthesis, characterization and luminescent properties of  $Eu^{3+}$ -doped gadolinium tungstate and molybdate phosphors:  $Gd(2-x)MO_6:Eu^{3+}$  ( $M=W, Mo$ ). *J Solid State Chem*. 2008;181:2845.
- Yue T, Baojiu C, Ruinian H, Jiashi S, Lihong C, Haiyang Z, et al. Optical transition, electron–phonon coupling and fluorescent quenching of  $La_2(MoO_4)_3:Eu^{3+}$  phosphor. *J Appl Phys*. 2011;109:3511.
- Dejneka M, Snitzer E, Riman RE. Blue, green and red fluorescence and energy transfer of  $Eu^{3+}$  in fluoride glasses. *J Lumin*. 1995;65:227.
- Brito HF, Malta OL, de Carvalho CA A, Menezes JFS, Souza LR, Fenaz LR. Luminescence behavior of Eu with thenoyltrifluoroacetone, sulfoxides and macrocyclics. *J Alloy Comp*. 1998;275–277:254.
- Xiangping L, Baojiu C, Rensheng S, Haiyang Z, Lihong C, Jiashi S, et al. Fluorescence quenching of 5DJ ( $J = 1, 2$  and 3) levels and Judd–Ofelt analysis of  $Eu^{3+}$  in  $NaGdTiO_4$  phosphors. *J Phys D Appl Phys*. 2011;33:5403.
- Nichkova M, Dosev D, Perron R, Gee SJ, Hammock BD, Kennedy IM.  $Eu^{3+}$ -doped  $Gd_2O_3$  nanoparticles as reporters for optical detection and visualization of antibodies patterned by microcontact printing. *Anal Bioanal Chem*. 2006;384:631.

46. Chen SC, Peron R, Dosev D, Kennedy IM. Time-gated detection of europium nanoparticles in a microchannel-based environmental immunoassay. *SPIE Proc SPIE 5275, BioMEMS and Nanotechnology 2004*, 186-196.
47. Weber MJ. Optical properties of ions in crystals. Edited by Crosswhite HM and Moos HW. New York: Wiley Interscience; 1976: 467–84.
48. Ribeiro SJL, Diniz REO, Messaddeq Y, Nunes LA, Aegerter MA.  $\text{Eu}^{3+}$  and  $\text{Gd}^{3+}$  spectroscopy in fluoroindate glasses. *Chem Phys Lett*. 1994;220:214.
49. Liqin L, Xueyuan C. Energy levels, fluorescence lifetime and Judd–Ofelt parameters of  $\text{Eu}^{3+}$  in  $\text{Gd}_2\text{O}_3$  nanocrystals. *Nanotechnology*. 2007;18:5704.
50. Chen X, Ma E, Liu G. Energy levels and optical spectroscopy of  $\text{Er}^{3+}$  in  $\text{Gd}_2\text{O}_3$  nanocrystals. *J Phys Chem C*. 2007;111:10404–11.
51. Balda R, Fernandez J. Visible luminescence in  $\text{KPb}_2\text{Cl}_5\text{Pr}^{3+}$  crystal. *Phys Rev B*. 1996;54:12076.
52. Zhao D, Qiao X, Fan X, Wang M. Local vibration around rare earth ions in  $\text{SiO}_2\text{-PbF}_2$  glass and glass ceramics using  $\text{Eu}^{3+}$  probe. *Phys B*. 2007;395:10.
53. Li XJ, Pun EYB, Zhang YY, Lin H. Radiative transitions of  $\text{Eu}^{3+}$  in non-crystalline alkali–alkaline–titanate film. *Phys B*. 2008;403:3509.
54. Saleem SA, Jamalalah BC, Mohan Babu A, Pavani K, Rama Moorthy L. A study on fluorescence properties of  $\text{Eu}^{3+}$  ions in alkali lead tellurofluoroborate glasses. *J Rare Earth*. 2010;28:189.
55. Babu P, Jayasankar CK. Optical spectroscopy of  $\text{Eu}^{3+}$  ions in lithium borate and lithium fluoroborate glasses. *Phys B Condens Matter*. 2000;279:262.
56. Grzyb T, Lis S. Structural and spectroscopic properties of  $\text{LaOF:Eu}^{3+}$  nanocrystals prepared by the sol gel Pechini method. *Inorg Chem*. 2011;50:8112.
57. Liu C, Liu J. Judd–Ofelt intensity parameters and spectral properties of  $\text{Gd}_2\text{O}_3\text{:Eu}^{3+}$  nanocrystals. *J Phys Chem B*. 2006;110(41):277–81.
58. Youssef ES, Damak K, Maalej R, Rüssel C. Thermal stability and UV–Vis–NIR spectroscopy of a new erbium-doped fluorotellurite glass. *Phil Mag*. 2012;92:899.

Submit your manuscript to a SpringerOpen<sup>®</sup> journal and benefit from:

- Convenient online submission
- Rigorous peer review
- Immediate publication on acceptance
- Open access: articles freely available online
- High visibility within the field
- Retaining the copyright to your article

---

Submit your next manuscript at ► [springeropen.com](http://springeropen.com)

---